RESEARCH ARTICLE | DECEMBER 13 2024

Analysis of the influence of abnormally grown grains on demagnetization behavior of FeNdB sintered magnets

Dominic Hohs ; Gerhard Martinek ; Ralf Loeffler; Dagmar Goll ; Gerhard Schneider

AIP Advances 14, 125212 (2024)
https://doi.org/10.1063/5.0242423

Analysis of the influence of abnormally grown grains on demagnetization behavior of FeNdB sintered magnets

Cite as: AIP Advances 14, 125212 (2024); doi: 10.1063/5.0242423
Submitted: 4 October 2024 • Accepted: 27 November 2024 •
Published Online: 13 December 2024

Dominic Hohs,[1,2,a)] Gerhard Martinek,[1] Ralf Loeffler,[1] Dagmar Goll,[1] and Gerhard Schneider[1,2]

AFFILIATIONS

[1] Materials Research Institute, Aalen University, Aalen, Germany
[2] Karlsruhe Institute of Technology, Karlsruhe, Germany

[a)] Author to whom correspondence should be addressed: dominic.hohs@hs-aalen.de

ABSTRACT

This study investigates the influence of abnormally grown grains on the magnetic properties of FeNdB sintered magnets. Specifically, the local demagnetization process caused by abnormally grown grains in the microstructure was analyzed by dynamic Kerr microscopy. The demagnetization process starts in large grains and has a strong influence on the surrounding microstructure. In a process similar to that described for non-magnetic inclusions or pores, the stray field of the already-demagnetized grain forms two areas with differing magnetic properties. A demagnetizing effect is found on the front faces of these grains while a stabilizing effect is found on the side faces. The negative influence of abnormal grain growth on the magnetic properties is also visualized.

INTRODUCTION

Hard magnetic materials are important functional materials for electric machines. FeNdB sintered magnets are the most widely used magnets due to their high remanence, high coercive field, and high magnetic energy product. High coercivity is important to stabilize the magnet against interfering fields in operation. By adding heavy rare earth elements such as Dy or Tb to the hard magnetic $Fe_{14}Nd_2B$ phase, its anisotropy field can be increased, which in turn boosts coercivity.[1] This may be realized by admixing these elements directly into the magnetic alloy from which the magnet will be produced. Unfortunately, this approach reduces the saturation polarization of the resulting $Fe_{14}(Nd,Dy,Tb)_2B$ phase, which consequently also decreases the remanence of the magnet. Another way is to introduce Dy and Tb subsequently via grain boundary diffusion treatment.[2] In addition, non-rare earth metals like Co and Cu can enhance the coercivity of the magnet by modifying the grain boundary phase.[3] In addition to chemical composition, the microstructure quality plays a crucial role with respect to the magnets aging and demagnetization behavior. On one hand, optimizing the grain size can result in higher coercivity obtained.[4–6] On the other hand, different types of defects in FeNdB sintered magnets, such as non-magnetic inclusions like RE-oxides or Fe_4NdB_4 phase agglomerates, can negatively influence the demagnetizing behavior and magnetic properties.

Durst *et al.*[7] describe the influence of non-magnetic inclusions and pores on the surrounding microstructure. According to Eq. (1), the stray field H_Z of a non-magnetic inclusion with radius a at an angle θ and distance d in direction z can be estimated. The strength of the stray field depends on the saturation polarization J_s of the surrounding microstructure:

$$\Delta H_Z(a+d) = -\frac{1}{3}\frac{a^3}{(a+d)^3} J_s\left(3\cos^2\theta - 1\right). \tag{1}$$

From Eq. (1), two characteristics become obvious. First, depending on the position of the stray field in relation to the pore, different effects on the magnetization behavior are expected (Fig. 1). Along the magnetization direction, the stray field of the pore has a demagnetizing effect. Perpendicular to the magnetization direction, the stray field of the pore has a stabilizing effect. Second, with increasing radius a of the non-magnetic inclusion, the stray field becomes more pronounced. This means that the risk of demagnetization increases with increasing defect size.

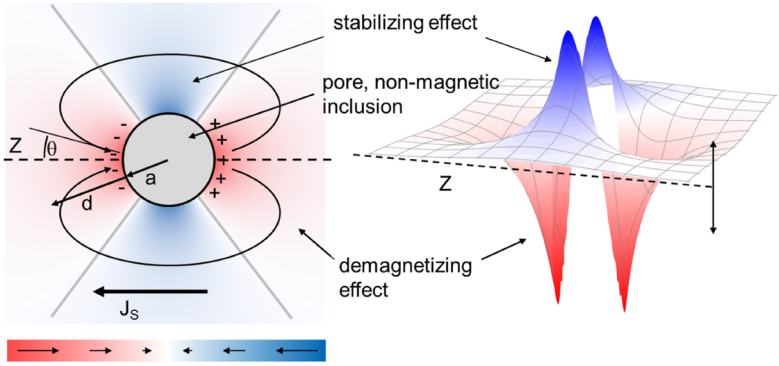

FIG. 1. Schematic illustration of a spherical pore or non-magnetic inclusion with the radius a in a magnetic matrix with saturation polarization J_s. The strength and orientation of the stray field depend on the distance $a + d$ and the angle θ [Eq. (1)]. This results in areas with a demagnetizing effect (red: stray field is antiparallel to the magnetization) and a stabilizing effect (blue: stray field is parallel to the magnetization direction). Illustration according to Ref. 7.

In addition to RE-oxides and η phase, a further defect that can occur is abnormal grain growth. When this occurs, some grains grow at the expense of neighboring smaller grains and can reach a few hundred microns.[8] Abnormal grain growth is favored by a small grain size and an inhomogeneous grain size distribution.[9] Residual hydrogen originating from the hydrogen embrittlement treatment, used to reduce the powder particle size during milling, can also lead to abnormal grain growth.[9] Finally, low oxygen levels can promote abnormal grain growth because fewer RE-oxides are formed, which act as grain growth inhibitors.[10] Due to their size, abnormally grown grains can be easily demagnetized. A lower resistance against demagnetization of abnormally grown grains compared to a fine matrix is also shown by Bittner *et al.*[11] by applying a magnetic field perpendicular to the easy axis. Similar to a non-magnetic inclusion as shown in Fig. 1, a fully demagnetized abnormally grown grain should produce an opposing magnetic stray field, which can affect the surrounding microstructure. To verify this, *in situ* analysis is needed. Combining an optical microscope (Kerr microscopy) with a magnetic field source enables the visualization of demagnetization processes in the microstructure of a magnet.[12–14] With this technique, the destabilizing potential of abnormal grain growth can be studied.

EXPERIMENTAL

For the experiment, a model FeNdB sintered magnet of composition Fe76.2-(Nd0.56Pr0.19 Ce0.25)14-B5.8-Co3.5-Cu0.1-Ga0.2-Al0.2 (at. %) was manufactured. The produced cast alloy was first crushed, then pulverized by hydrogen embrittlement, and subsequently jet milled. The resulting powder was pressed in the presence of a 2 T magnetic field, and the obtained magnetically textured green body was sintered at 1010 °C for 2 h to provoke abnormal grain growth. The post-annealing was carried out at 800 and 500 °C for 2 h each.

Magnetic properties

The magnetic properties of the sample, as well as the properties of a commercial reference magnet (grade N38), were measured in a hysteresis graph (Magnet-Physik Dr. Steingroever GmbH) at room temperature. The macroscopic characteristics (coercivity, H_C, and remanence, B_r) as well as the curve shape (squareness) were determined from the hysteresis loop.

X-ray microscopy

The distribution of abnormally grown grains was determined by 3D x-ray microscopy. A sample with the dimensions of 7.9 × 3.6 × 11.9 mm^3 was analyzed using a high-resolution 3D x-ray microscope (Zeiss Xradia Versa 610). An acceleration voltage of 160 kV and a power of 25 W was used to achieve a voxel size of 15.5 μm.

Microstructure analysis

For the microstructure and optical demagnetization analysis, a sample with the dimensions 3.7 × 3.0 × 2 mm^3 was taken from the sintered magnet and polished for microscopic analysis. The optical light microscope used was a Carl Zeiss Imager.Z2 Vario with an electromagnet and light source from evico magnetics GmbH. The magneto-optical Kerr effect (MOKE) was used to visualize the magnetization. The image acquisition condition was set so that only the in-plane magnetization was visualized.[13] For further contrast enhancement, a difference imaging method was used. At the beginning of the demagnetization sequence, a reference image of the fully saturated state was taken, containing only the sample's topography contrast. Using additional imaging processing, this topography contrast was then subtracted from each acquired Kerr image, so that the image's magnetic contrast was considerably intensified.[15] Areas of original magnetization appear gray, while demagnetized areas appear bright. Before recording the demagnetization sequence, the sample was magnetized using a 7 T pulse magnetizer (Magnet-Physik Dr. Steingroever GmbH). The sample was mounted in the electromagnet of the *in situ* microscope and magnetized to +700 mT. A reversed field was subsequently applied until all grains were completely magnetized in the opposite direction. The range of the recording (H_{extern}) was from +300 to −400 mT, with a resolution of 10 mT. The resulting image sequence then was transferred to a false-color image with a rainbow scheme according to Hohs *et al.*[16]

In addition, a 2D simulation of the magnetic flux of a fully saturated matrix and a fully demagnetized grain was created with Simcenter MAGNET. Both the grain shape and the orientation of the easy axis were modeled according to the micrographs. The matrix was set to a homogeneous area with a polarization of 1.24 T according to the hysteresis graph measurement. The polarization of the grain was set to 1.61 T according to the properties of an $Fe_{14}Nd_2B$ single crystal.[17] Based on the microscopic observation,

the properties of the grain were set to a soft magnet with uniaxial anisotropy.

RESULTS

Figure 2(a) shows the second quadrant of the demagnetization curve of the sample with abnormal grain growth and the commercial N38 reference magnet. Both magnets achieve the required coercivity of >955 kA/m and the minimal remanence of 1.22 T, which is required for a magnet with a maximal operating temperature of 80 °C. The magnet with abnormal grain growth shows a coercivity of 997 kA/m, while the reference magnet shows 1114 kA/m. However, differences in the slope of the curve are visible. Starting at a remanence of 1.24 T, the polarization significantly decreases with increasing counter field strength in the sample. In the horizontal part of the demagnetization loop, the average demagnetization rate for the magnet with abnormal grain growth is −0.2 mT/kAm^{-1} (magnetic susceptibility χ_R = 0.25). The loss of polarization for the commercial reference magnet is −0.04 mT/kAm^{-1} (χ_R = 0.05), which is therefore four times lower. For the calculated H_{D5} of 930 kA/m, the drop of polarization in the magnet with abnormal grain growth is about 18% (1.04 T). Figure 2(b) shows the linear part of the curve in the second quadrant in more detail. While the slope of the demagnetization curve of the reference magnet increases slightly at higher magnetic fields, the curve of the magnet with abnormal grain growth shows a kink at ~420 kA/m. At this point, the demagnetization rate decreases slightly. According to Equation (2),

$$\frac{J_r - J_{420\mathrm{kA/m}}}{2J_r} = V_{dem}, \tag{2}$$

where the loss of polarization (1.158 T at 420 kA/m) can be calculated for a demagnetized volume of 3.3%. In addition, a step in the demagnetization curve of the reference magnet at 100 kA/m is visible, which can be explained by the demagnetization of the surface.[18]

The x-ray microscopy analysis of the magnet reveals the volumetric distribution of the abnormally grown grains. The difference in the average radiodensity of the singular large ϕ grain and the matrix (a patchwork of smaller ϕ grains surrounded by a more radiodense grain boundary phase) results in a sufficiently large contrast in the tomographic image. In the cross-section [Fig. 3(a)], abnormally grown grains are visible as dark spots. This allows the detection of abnormally grown grains by image analysis and quantification of their distribution in the magnet. In the 3D-volume image, all abnormally grown grains are separated by AI-supported segmentation and color-coded according to their size [Fig. 3(b)]. For better visualization, the matrix is displayed semi-transparently. Abnormal grain growth occurs homogeneously throughout the sample volume. For the quantification, only grains over 150 μm (10 times the voxel size of 15 μm) are considered [Fig. 3(c)]. From this, the grain size distribution of abnormally grown grains is calculated. The total volume fraction of large grains is 2.2% of the sample volume. The volume-weighted mean grain diameter of abnormally grown grains is D_{50} = 284 μm, with a few grains exceeding 600 μm.

For investigating the influence of abnormally grown grains on the demagnetization behavior of the microstructure, a grain with a diameter of 250 μm was examined in detail using materialographic target preparation and high-resolution *in situ* Kerr microscopy. A fully magnetized polished microsection of the magnet was exposed to a systematically varied external magnetic field, starting at +700 mT and decreasing to −400 mT. Selected images of the acquired demagnetization sequence are shown in Fig. 4. Here, the easy axis of the magnetization and the direction of the external magnetic field are aligned parallel to each other and lie in the image plane as indicated by the yellow arrows. Starting at +700 mT, no demagnetization was visible down to +300 mT [Fig. 4(a)]. In the range from +300 to +100 mT, the first reversed domains (bright) appeared in the abnormally grown grain [Fig. 4(b)]. A few grains of the matrix, especially at the edges of the abnormally grown grain (highlighted by the red circles), also became demagnetized. With further reduction of the external magnetic field to 0 mT [Fig. 4(c)], the number of reversed domains in the abnormally grown grain increased, which was now mostly demagnetized. In addition, the proportion of demagnetized grains near the large grain increased, as marked by red circles. Since no external field is applied, Fig. 4(c) also shows the state of pure self-demagnetization. From this point forward, a magnetic counter field was applied. This led to an expansion of demagnetized grains in the matrix at the front faces of the abnormally grown grain. Figure 4(d) shows the demagnetization state at −100 mT. The demagnetized

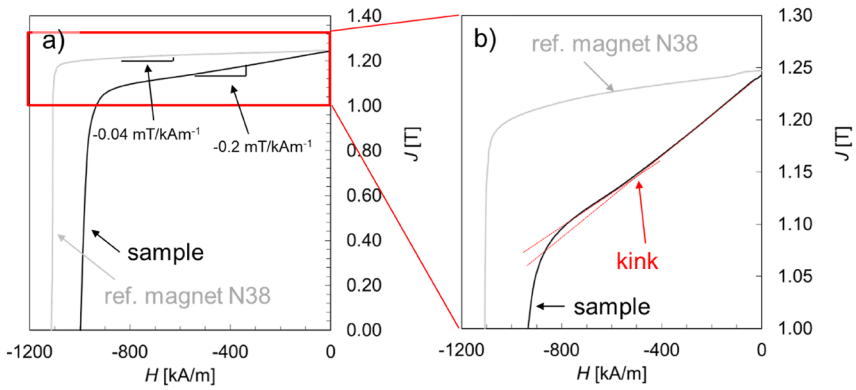

FIG. 2. (a) Different slopes in the second quadrant of the hysteresis loop for the commercial reference magnet N38 and the magnet with abnormal grain growth. (b) The magnet with abnormal grain growth shows a kink in the demagnetization curve at −420 kA/m, at which point the demagnetization rate decreases slightly.

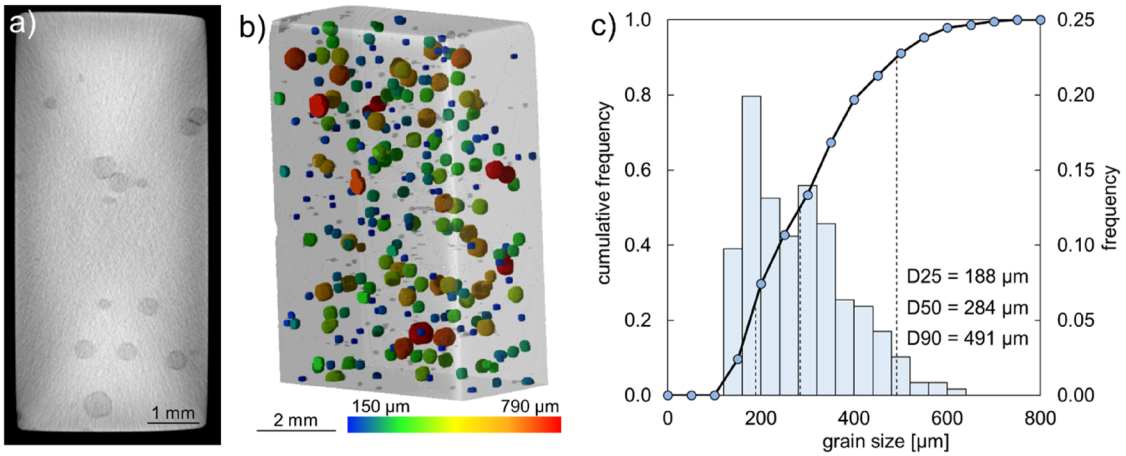

FIG. 3. X-ray microscopy scan of a magnet with detected abnormally grown grains. In the cross-section of the volume image (a), abnormally grown grains are visible as dark spots. In the corresponding false color image (b), abnormally grown grains are color-coded according to their grain size. The abnormally grown grains are homogeneously distributed in the sample. The computed grain size distribution shows that most of the grains have a diameter of 200–400 μm (c).

areas are marked with red circles. The demagnetization process continued until the uninfluenced matrix was fully demagnetized. At −200 mT [Fig. 4(e)], only the areas at the side face of the grain were still in the initial magnetization state, marked with blue circles. These areas shrank with increasing counter field [Fig. 4(f), −280 mT]. A magnetic field of −350 mT was needed for full demagnetization of these areas. Differences in the demagnetization behavior are visible. While demagnetization of the large grain occurred via the multidomain state, smaller grains, often as clusters, immediately switched their magnetization completely along the magnetization

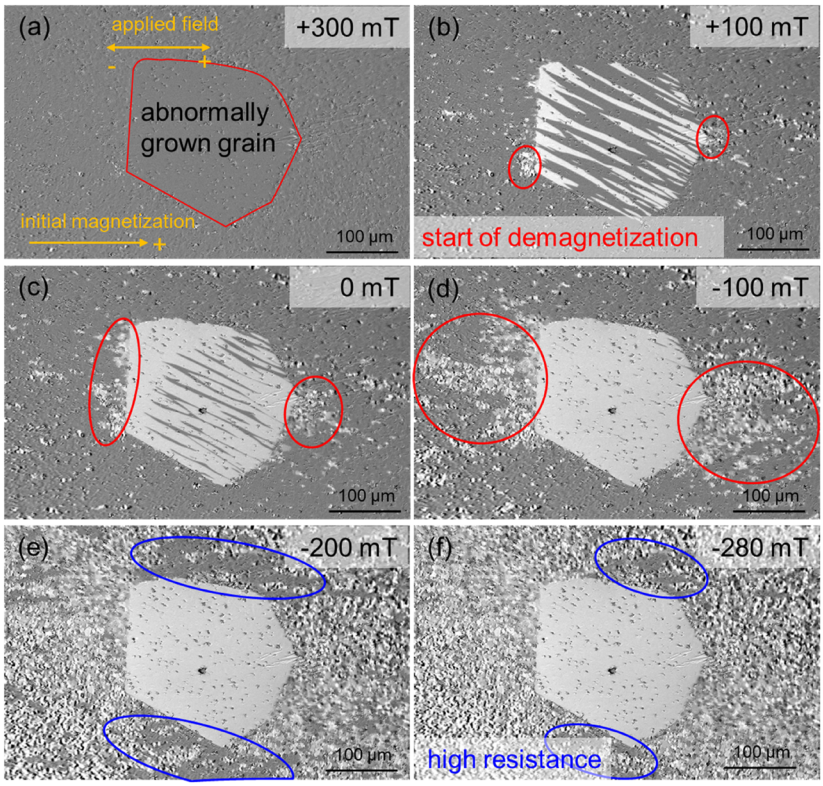

FIG. 4. Demagnetization sequence of an abnormally grown grain and the surrounding microstructure, captured by *in situ* Kerr microscopy at various applied fields. Starting at +300 mT (a), the demagnetization begins in the abnormally grown grain. With decreasing external magnetic field (b) and (c), the abnormally grown grain and areas (red) surrounding the grain are demagnetizing. While applying a field in the opposite direction (d)–(f), the demagnetization process continues; however, the areas on the side face of the grain (blue) still remain in the initial state of magnetization.

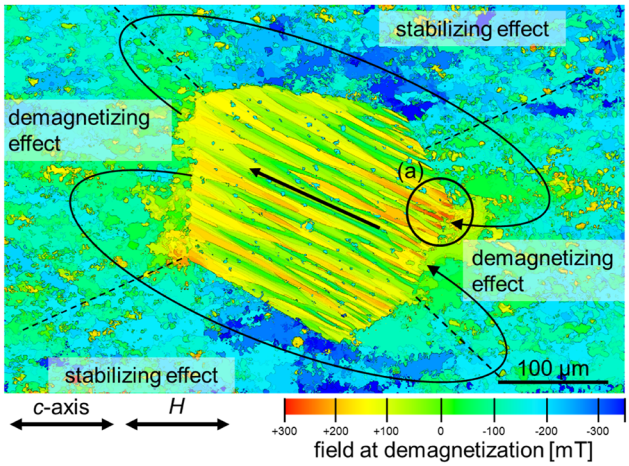

FIG. 5. The demagnetization map of the abnormally grown grain colored according to the applied field strength at the time of demagnetization. The demagnetization starts in the abnormally grown grain (red to yellow) and continues in the matrix at the front face of the grain. Grains at the side face are demagnetizing at the end (blue). From this, two areas can be identified, one with a demagnetizing and one with a stabilizing effect.

direction. It can also be seen that regions on the front side of the grain (red) demagnetized early, while the regions on the side surface were demagnetized last.

For a better visualization, the applied field at the time of demagnetization was transferred into a false-color image (Fig. 5). This image shows that the beginning of the demagnetization process starts in the large grain, more precisely at the corner (a) at an applied field of +300 mT. The first stripe domains appearing are colored in red. Further demagnetization occurs in the areas colored from yellow to green, corresponding to an external magnetic field of +300 to 0 mT. The microstructure at the front face of the grain mostly shows yellow and green colors, equivalent to a magnetic field of +150 to −150 mT. The microstructure at the side surfaces demagnetized at a field of −200 to 350 mT and is thus colored in blue. From the illustration, two areas in the surrounding microstructure can be identified. At the front face area, demagnetization at low fields is visible (a), while at the side faces, the demagnetization finished last (−350 mT), as indicated by the blue color.

For a better interpretation of the demagnetization process observed by Kerr microscopy, a simplified model of the demagnetization fields around the grain was simulated. Due to the observed behavior, the abnormally grown grain is defined as a soft magnetic component with high anisotropy. The anisotropy axis is tilted by 15° (as estimated by the orientation of the stripe domains seen in the micrograph) against the magnetization direction.

Figure 6 shows the magnetic state without an external field. The combination of the demagnetizing field of the sample and the local demagnetizing field of the grain means that the grain is already clearly magnetized in the opposite direction at $H_{ext} = 0$. This is in line with the observation in Fig. 4(c). In Fig. 6(a), the domain structure from Fig. 4(c) was overlaid. In areas with a high B value in the negative direction (red areas), no domains are visible. Only in the middle of the grain, where B is around 0, domains are visible.

At this point, the abnormally grown grain, acting like a soft magnetic grain, is nearly fully magnetized in the opposite direction and will influence its surroundings. In Fig. 6(b), the demagnetization field is shown. An increase in the demagnetization field at the front faces of the grain (red) is visible. At the side faces of the grain, the demagnetization field is lowered (blue). Both effects are weakened with increasing distance from the grain.

DISCUSSION

Different analysis methods were used to analyze the influence of abnormal grain growth on the demagnetization behavior of FeNdB sintered magnets, spanning from global magnetic properties to quantitative visualization of local demagnetization behavior of the microstructure. According to Ramesh *et al.*,[5] the presence of abnormally grown grains is expressed in the hysteresis loop by an early and high loss of magnetization in the linear region accompanied by pronounced kinks. The drop in polarization indicates a partial

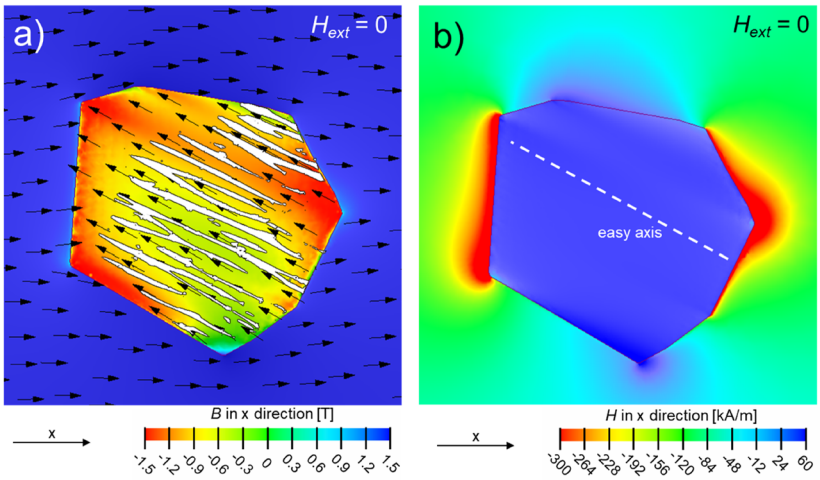

FIG. 6. Magnetic simulation of the abnormally grown grain in a homogeneous matrix. The properties of the abnormally grown grain are assumed to be those of a soft magnet with a high anisotropy (permeability parallel: 100; perpendicular: 1). The B-field simulation shows that the magnetization direction of the grain pinpoints in the opposite direction. The domain structure obtained from Fig. 4(c) is overlaid in (a) for a better visualization. Those domains are only in areas with B values around 0, but not in the areas with a high negative B value (red). (b) The demagnetization field is the strongest at the pole faces and the lowest at the side faces of the grain.

demagnetization of the sample before the coercivity of the material is reached. However, the coercivity H_{cj} itself is not significantly influenced by the presence of abnormally grown grains. All these features can be clearly detected in the acquired hysteresis loop of the model sample. Both an early and steady steep drop of magnetization as well as a kink are observed in Figs. 2(a) and 2(b). Magnetization drops especially sharply at the coercivity [Fig. 2(a)], and the sample loses 18% of polarization when reaching H_{D5} (930 kAm^{-1}). The loss of polarization in the linear section of the hysteresis of the investigated sample is about 0.2 mT/kAm^{-1} (χ_R = 0.25) and of the reference magnet without abnormal grain growth is 0.04 mT/kAm^{-1} (χ_R = 0.05). This is similar to the hysteresis loops from Ramesh *et al.*,[5] which show a loss of polarization of 0.05 mT/kAm^{-1} (χ_R = 0.06) and 0.3 mT/kAm^{-1} (χ_R = 0.38) for magnets containing 0.5 and 4 vol. % of abnormally large grains, respectively. From the height of the drop at 420 kA/m, a demagnetized volume of 3.3% can be calculated for the magnet with abnormal grain growth. Using x-ray microscopy, a volume fraction of 2.2% could be determined. These results are in the same order of magnitude and fit together very well. From the x-ray analysis, the average size of the abnormally grown grains was determined to be 284 μm, with a few grains exceeding 600 μm.

The demagnetization mechanism at the microstructure level was investigated to better understand the macroscopic demagnetization behavior seen in the hysteresis loop. Therefore, an abnormally grown grain with a diameter of 250 μm (close to the average of 284 μm) was examined in a demagnetizing magnetic field. This is illustrated in Fig. 4, which shows that demagnetization starts in the abnormally grown grain. This can be explained by a reduced nucleation energy. Nucleation of reverse domains typically starts at defects in the grain boundaries where the required nucleation energy is lower. Due to the larger surface area of the abnormally grown grain, the probability of faults and defects occurring in the grain boundary is also higher for this grain.[5,19]

In the microscope, it can be seen that the first appearance of reverse domains is in the right corner of the grain (Fig. 5). The experimental observations can be explained by magnetic simulation; for example, Fig. 6(a) reveals that this area also exhibits the highest magnetic flux within the grain without an external field. Comparing the calculated magnetic flux [Fig. 6(a)] with the domain structure [Fig. 4(c)] without an external field, it can be seen that the areas with the highest flux are the areas that first show a state without reverse domains. Only in the center do a few reverse domains remain. The following demagnetization process in this grain continues through domain wall movement until it is fully demagnetized. Its magnetization direction is now pointing in the opposite direction of the initial magnetization of the matrix. This generates a stray field, which is at the front face of the grain, also pointing in the opposite direction. As clearly seen in the simulation [Fig. 6(b)], those areas are showing the highest demagnetization fields (red). This is enough to reach the coercivity field strength of the matrix grains, which leads to a local demagnetization (Fig. 4). The simulated demagnetization field [Fig. 6(b)] is in agreement with the start of the observed demagnetization [Fig. 4(a) red circles] in the demagnetization sequence. The high stray field at the corners of the abnormally grown grain forces the microstructure grains to change their magnetization direction. With increasing external magnetic field, the demagnetization propagates deeper into the matrix, but only at the front faces of the grain due to the weakening effect of the stray field generated by the large grain. At the side face of the grain, the stray field aligns with the initial magnetization of the matrix. This is confirmed by the reduction of the expected demagnetization field [blue areas, Fig. 6(b)]. This leads to a local stabilizing effect of these matrix grains. Both the demagnetization and stabilization effects decline with increasing distance to the abnormally grown grain, as is observed in Figs. 5 and 6. This is similar to the effect of nonmagnetic inclusions calculated by Durst *et al.*[7] While they find reverse domains appearing in grains connected to the defect, we observed whole clusters of grains changing their magnetization direction simultaneously. This can be explained by the varying size of the observed defects. The abnormally grown grain is much bigger than the average grain size of the matrix, while the non-magnetic inclusion is in the order of magnitude of matrix grains. Although the simulation model is very simplified, it gives a quite good illustration of the magnetic state of the grain and its surroundings.

The difference between the observed demagnetization with MOKE and the hysteresis loop is also observed elsewhere[20] and explained by self-demagnetization effects at the surface. A weakening of the magnetic hardness at the surface is expected due to damaged surface grains and missing grain boundary phase.[11,20,21] In addition, the observation of the demagnetization behavior under the microscope took place in an open magnetic loop. Therefore, a demagnetizing factor of 0.25, due to the given sample geometry, will affect the demagnetization. This will shift the observed demagnetization effect to lower fields but will not influence the observed phenomena of demagnetization and stabilization areas induced by the defect.

CONCLUSION

In this study, demagnetization processes at defects were visualized in the microstructure and connected to changes in macroscopic properties. On a macroscopic scale, it has been shown that the presence of only 2 vol. % of abnormally grown grains can lead to an early loss of polarization during demagnetization. Through visualization of the demagnetization process in the microstructure, it was possible to connect the early drop of polarization (0.2 mT/kAm^{-1}) before reaching coercivity with demagnetization occurring at abnormally grown grains and their surrounding matrix. The visualization of the demagnetization process also confirms two distinct effects around the defect: a demagnetizing effect at the front faces and a stabilizing effect at the side faces of the defect. It was shown that a fully demagnetized grain behaves similarly to a non-magnetic inclusion. In addition, the Kerr observation is in good agreement with a simplified magnetic simulation model of the defect. This confirms that the observed early demagnetization is indeed caused by the stray field induced by the abnormally grown grain. While the coercivity itself may not be strongly influenced by abnormal grain growth, early demagnetization leads to a strong loss of the maximum energy product and a reduction of the maximum working temperature. To prevent magnetic aging, defects such as abnormal grain growth must be avoided. The dynamic Kerr microscopy provides a

deeper understanding of the influence of defects on demagnetization behavior.

ACKNOWLEDGMENTS

The authors would like to thank Marius Böttle (Aalen University) for assistance in sample synthesis and Tim Schubert (Aalen University) for assistance in x-ray microscopy analysis.

This research was funded by the German Federal Ministry of Education and Research (BMBF) within the scope of the project SmartMAG (Grant No. 13FH4I08IA) as part of the research program FH-Impuls.

The Kerr microscope was funded by the German Research Foundation (DFG) under Grant No. 413993866. Publication funded by Aalen University of Applied Sciences.

AUTHOR DECLARATIONS

Conflict of Interest

The authors have no conflicts to disclose.

Author Contributions

Dominic Hohs: Conceptualization (equal); Data curation (lead); Formal analysis (equal); Investigation (lead); Methodology (equal); Software (equal); Validation (equal); Visualization (lead); Writing – original draft (lead); Writing – review & editing (equal). **Gerhard Martinek**: Formal analysis (equal); Investigation (equal); Methodology (equal); Software (equal); Validation (equal); Visualization (equal); Writing – original draft (equal); Writing – review & editing (equal). **Ralf Loeffler**: Methodology (equal); Validation (equal); Writing – original draft (equal); Writing – review & editing (equal). **Dagmar Goll**: Conceptualization (equal); Funding acquisition (equal); Methodology (equal); Project administration (equal); Resources (equal); Supervision (equal); Writing – original draft (equal); Writing – review & editing (equal). **Gerhard Schneider**: Conceptualization (equal); Funding acquisition (equal); Methodology (equal); Project administration (equal); Resources (equal); Supervision (equal); Writing – original draft (equal); Writing – review & editing (equal).

DATA AVAILABILITY

The data that support the findings of this study are available within the article.

REFERENCES

[1] M. Sagawa, S. Hirosawa, H. Yamamoto, S. Fujimura, and Y. Matsuura, Jpn. J. Appl. Phys. **26**, 785 (1987).
[2] K. Hirota, H. Nakamura, T. Minowa, and M. Honshima, IEEE Trans. Magn. **42**, 2909 (2006).
[3] A. S. Kim and F. E. Camp, J. Appl. Phys. **79**, 5035 (1996).
[4] K. Uestuener, M. Katter, and W. Rodewald, IEEE Trans. Magn. **42**, 2897 (2006).
[5] R. Ramesh, G. Thomas, and B. M. Ma, J. Appl. Phys. **64**, 6416 (1988).
[6] K. Hono and H. Sepehri-Amin, Scr. Mater. **67**, 530 (2012).
[7] K.-D. Durst, H. Kronmüller, and G. Schneider in *Proceedings of the 9th International Workshop on Rare-Earth Magnets and their Applications, 31 August–2 September 1987 and 5th International Symposium on Magnetic Anisotropy and Coercivity in Rare-Earth -Transition Metal Alloys, 3 September 1987 DPG-GMBH* (DPG-GmbH, Bad Soden, 1987), p. 209.
[8] N. C. Liu and A. S. Kim, J. Appl. Phys. **67**, 4629 (1990).
[9] F. Vial, E. Rozendaal, and M. Sagawa, "Improvement of the microstructure and magnetic properties of sintered NdFeB permant magnets," in *Proceedings of the 15th International Workshop on Rare-Earth Magnets and their Applications* (Werkstoff-Informationsgesellschaft, 1998), p. 401.
[10] M. R. Corfield, I. R. Harris, and A. J. Williams, J. Alloys Compd. **463**, 180 (2008).
[11] F. Bittner, T. G. Woodcock, L. Schultz, C. Schwöbel, O. Gutfleisch, G. A. Zickler, J. Fidler, K. Üstüner, and M. Katter, J. Magn. Magn. Mater. **426**, 698 (2017).
[12] J. Pastushenkov, K.-D. Durst, and H. Kronmüller, Phys. Status Solidi A **104**, 487 (1987).
[13] I. V. Soldatov and R. Schäfer, Rev. Sci. Instrum. **88**, 73701 (2017).
[14] M. Takezawa, Y. Ichihara, Y. Morimoto, and J. Yamasaki, IEEE Trans. Magn. **45**, 4439 (2009).
[15] A. Hubert and R. Schaefer, *Magnetic Domains. The Analysis of Magnetic Microstructures* (Springer, Berlin, Heidelberg, 1998).
[16] D. Hohs, S. Klett, R. Löffler, F. Trier, D. Goll, and G. Schneider, Pract. Metallogr. **60**, 37 (2022).
[17] S. Hirosawa, Y. Matsuura, H. Yamamoto, S. Fujimura, M. Sagawa, and H. Yamauchi, J. Appl. Phys. **59**, 873 (1986).
[18] D. Givord, P. Tenaud, and T. Viadieu, J. Appl. Phys. **60**, 3263 (1986).
[19] H. Kronmüller and M. Fähnle, *Micromagnetism and the Microstructure of Ferromagnetic Solids* (Cambridge University Press, Cambridge, 2003).
[20] F. Chen, L. Zhang, and Y. Jin, J. Appl. Phys. **124**, 53902 (2018).
[21] T. Fukagawa and S. Hirosawa, J. Appl. Phys. **104**, 13911 (2008).